Bioactive Materials 34 (2024) 150–163

Contents lists available at ScienceDirect

Bioactive Materials

journal homepage: www.keaipublishing.com/en/journals/bioactive-materials

Advancing homogeneous networking principles for the development of fatigue-resistant, low-swelling and sprayable hydrogels for sealing wet, dynamic and concealed wounds in vivo

Yi Zhang [a,1], Yanjun Pan [b,1], Ronghang Chang [a], Kangli Chen [a], Kun Wang [a], Haoqi Tan [c], Meng Yin [b,**], Changsheng Liu [a], Xue Qu [a,d,e,*]

[a] Key Laboratory for Ultrafine Materials of Ministry of Education, School of Material Science and Engineering, Frontiers Science Center for Materiobiology and Dynamic Chemistry, East China University of Science and Technology, Shanghai 200237, China
[b] Department of Cardiothoracic Surgery, Shanghai Children's Medical Center, School of Medicine, Shanghai Jiao Tong University, 1678 Dong Fang Road, Shanghai 200127, China
[c] Suzhou Innovation Center of Shanghai University, Shanghai University, Suzhou 215000, Jiangsu, China
[d] Wenzhou Institute of Shanghai University, Wenzhou, 325000, China
[e] Shanghai Frontier Science Center of Optogenetic Techniques for Cell Metabolism Shanghai, 200237, China

ARTICLE INFO

Keywords:
Sprayable hydrogel sealants
Homogeneous network
Fatigue-resistance
Low swelling
Wet dynamic and concealed wound

ABSTRACT

Effective sealing of wet, dynamic and concealed wounds remains a formidable challenge in clinical practice. Sprayable hydrogel sealants are promising due to their ability to cover a wide area rapidly, but they face limitations in dynamic and moist environments. To address this issue, we have employed the principle of a homogeneous network to design a sprayable hydrogel sealant with enhanced fatigue resistance and reduced swelling. This network is formed by combining the spherical structure of lysozyme (LZM) with the orthotetrahedral structure of 4-arm-polyethylene glycol (4-arm-PEG). We have achieved exceptional sprayability by controlling the pH of the precursor solution. The homogeneous network, constructed through uniform crosslinking of amino groups in protein and 4-arm-PEG-NHS, provides the hydrogel with outstanding fatigue resistance, low swelling and sustained adhesion. In vitro testing demonstrated that it could endure 2000 cycles of underwater shearing, while in vivo experiments showed adhesion maintenance exceeding 24 h. Furthermore, the hydrogel excelled in sealing leaks and promoting ulcer healing in models including porcine cardiac hemorrhage, lung air leakage and rat oral ulcers, surpassing commonly used clinical materials. Therefore, our research presents an advanced biomaterial strategy with the potential to advance the clinical management of wet, dynamic and concealed wounds.

1. Introduction

Hydrogel sealants are employed as noteworthy alternatives to traditional surgical sutures and staples owing to their capacity to create a moist environment, absorb tissue exudates, and act as a barrier against microbial invasion [1–3]. Conventional methods of delivering hydrogel to wounds typically involve injection [4,5] and patching [6]. Nonetheless, these techniques may be unsuitable for some practical treatments that are challenging to swiftly pinpoint the wound and confined by surgical visuality, like oral ulcers, pulmonary leakage and posterior cardiac anastomotic procedures [7–9]. In contrast, spraying emerges as an efficient approach to be applied in concealed wounds, which permits the broad application of hydrogel across the wound area without precise locations [10–12]. However, the effectiveness of sprayable hydrogel sealants hinges on specific attributes. Foremost among these is the imperative of a high fluidity in the precursor solution, facilitating effective mixing and smooth spraying [13,14]. Moreover, fast gelation is essential to ensure that the solution solidifies promptly upon contact

Peer review under responsibility of KeAi Communications Co., Ltd.
* Corresponding author. East China University of Science and Technology, No 130, Meilong Road, Shanghai, China.
** Corresponding author.
E-mail addresses: 454982313@qq.com (H. Tan), yinmengmdphd@163.com (M. Yin), quxue@ecust.edu.cn (X. Qu).
[1] Y. Zhang, Y. J. Pan contributed equally to this article.

https://doi.org/10.1016/j.bioactmat.2023.12.002
Received 26 September 2023; Received in revised form 14 November 2023; Accepted 1 December 2023

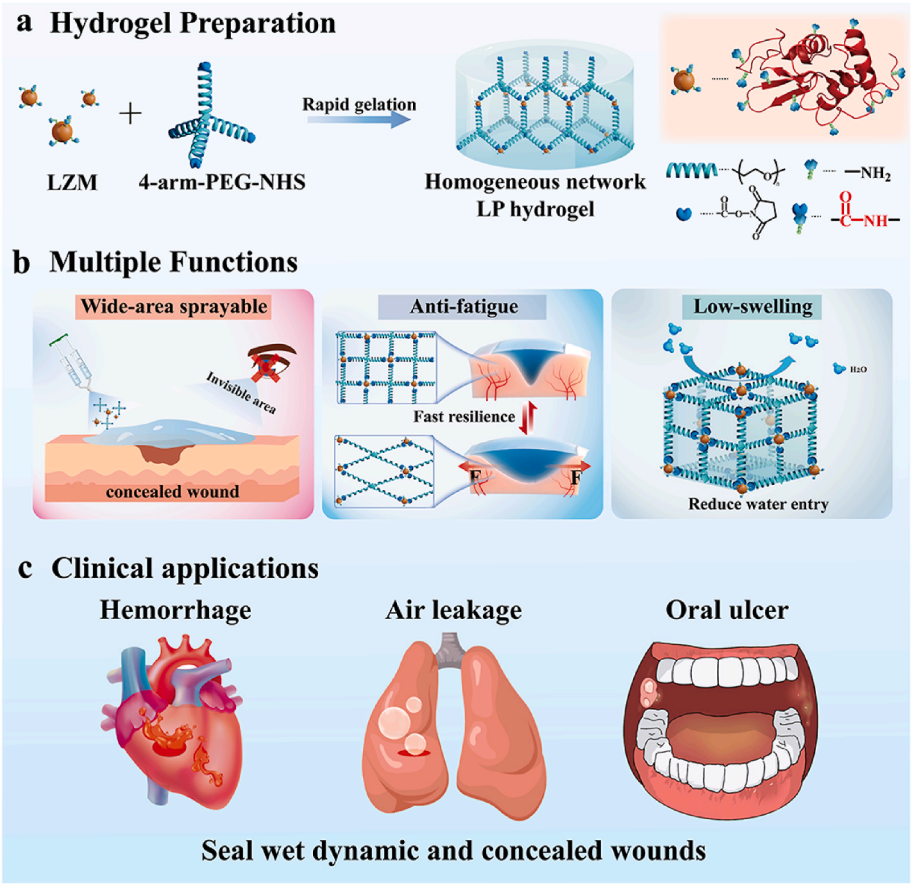

Scheme 1. Construction of Lysozyme/4-arm-PEG (LP) hydrogel sealant with homogenous network characteristics and its multiple functions and potential clinical applications. (a) The LP hydrogel with a homogeneous network is prepared by crosslinking lysozyme with spherical structure and 4-arm-PEG-NHS with orthotetrahedral structure (LZM's 3D structure model sourced from the Protein Data Bank shows externally distributed amine groups originating from arginine). Rapid gelation can be achieved by using an appropriate borax buffer solution to promote the deprotonation of amine groups. (b) The LP hydrogel exhibits wide-area sprayable, anti-fatigue and low-swelling properties. The short gelation time imparts wide-area sprayability to the hydrogel for rapidly sealing concealed wounds. The homogenous network eliminates imperfections network and evenly distributes stress among all chains, leading to the rapid resilience of hydrogel and imparting anti-fatigue properties to it. The structure of the network remains stable during the swelling process, resulting in the low swelling characteristic. Consequently, (c) LP hydrogel has great potential for clinical therapy for wet, dynamic and concealed wounds, including cardiac hemorrhage, lung air leakage, and oral ulcers.

with the target tissue, thereby averting off-target [15,16]. One practical approach to accelerating the gelation of an amino bond-driven hydrogel is elevating the solute concentration in the precursor solution [17]. Nonetheless, this method concurrently results in heightened viscosity, potentially impeding the sprayability. In our prior investigations, a straightforward technique was developed for accelerating gelation by altering the pH of the precursor solution, all while keeping its composition and fluidity unchanged [18]. Although substantial progress has been made in sprayable hydrogel sealants, revealing notable therapeutic promise concerning external wounds [19,20], the consideration of fatigue resistance and swelling resistance in these hydrogels is frequently neglected [21,22]. The application of hydrogels with high hysteresis in dynamic tissue may result in dislocation or complete detachment from the wound due to frequent tissue deformation [23]. Additionally, severe swelling compromises mechanical performance and adhesion, exacerbating the compression of adjacent tissue [24–26]. Therefore, the dynamic and wet environment imposes heightened expectations on the overall performance of hydrogels, with particular emphasis on fatigue resistance and swelling inhibition.

Currently, the strategies employed to enhance the fatigue resistance of hydrogels include the introduction of micelles [27,28], chain entanglement [29,30], and the formation of a homogeneous network [31–33]. Micelles as dynamic macromolecular cross-linkers within hydrogels. This integration imparts notable fatigue resistance to the hydrogels, primarily attributed to the swift reorganization and recuperation of the micelles during deformation [34]. However, the inherent instability of micelles contributes to the loosening of the hydrogel's network structure during the swelling, leading to excessive swelling [34,35]. Chain entanglement arises when flexible molecular chains with high molecular weights and low chemical cross-linking points, allowing external forces to be transferred among the entangled chains [36]. However, a low cross-linking density inevitably results in a high swelling, which is considered undesirable for in vivo applications. Additionally, the entanglement-induced viscous precursor solution poses a challenge to spraying [37,38]. The presence of a homogeneous network serves to alleviate stress concentration occurrences by eradicating microscopic imperfections, consequently enhancing the hydrogel's ductility [39]. Furthermore, hydrogels with a homogeneous network demonstrate fatigue resistance, attributed to the swift absorption and release of energy through the rapid conformational transitions within all constituent chains and no network imperfection consumes energy [40,41]. Additionally, the structurally stable homogeneous network efficiently restricts water entry, consequently leading to low swelling [42]. In conclusion, the introduction of a homogeneous network has the potential to augment the fatigue resistance and swelling resistance of the conventional hydrogel.

Early studies have proposed that the orthotetrahedral structure of the 4-arm- poly (ethylene glycol) (PEG) plays a crucial role in

establishing spatial homogeneity within PEG hydrogels [43]. This homogeneity is conducive to the creation of a network closely resembling an ideal homogeneous network in which the chains connecting each cross-linking point possess identical lengths and undergo simultaneous extension and rupture [44–46]. However, despite the presence of such a homogeneous network, full PEG hydrogels still demonstrate pronounced swelling resulting from the combined effects of their flexible molecular chains, hydrophilicity, steric hindrance effect, and molecular weight [47]. Low swelling is crucial for the internal application of hydrogel sealants [48]. Traditional strategies encompass enhancing crosslinking density [4,49]. Nevertheless, the strategy may lead to heightened hydrogel stiffness, thereby undermining its adaptability.

Lysozyme (LZM) is a type of enzyme protein that is naturally present in many organisms and serves essential biological functions [50]. The molecular conformation of lysozyme is relatively stable, enabling it to maintain its functionality under various environmental conditions [51]. Lysozyme has been used in our hydrogel constructions, mainly aiming to enhance the biological performance of hydrogels [52,53]. In this investigation, we focus on the spherical protein structure characteristics of lysozyme with evenly distributed reactive amine groups [51] and anticipate that this may facilitate constructing a homogenous network with the orthotetrahedral 4-arm-PEG-NHS. Additionally, due to the less extensible molecular chains of globular proteins, the homogenous networks LZM participates in the building are anticipated more compact than pure PEG hydrogel, which can further alleviate swelling in water. Scheme 1 illustrates the material preparation and its multiple functions. Scheme 1 (a) shows a homogenous network of LZM/4-arm-PEG (LP) composing LZM and 4-arm-PEG-NHS can be prepared via amide groups formation. Rapid gelation can be achieved by using an appropriate buffer solution to promote the deprotonation of amine groups. Scheme 1 (b) depicts the multiple functions of the LP hydrogel. The precursor solutions of LZM and PEG can be sprayed across a substantial area without pinpointing, subsequently solidifying in situ upon wounds. Secondly, the LP hydrogel exhibits commendable fatigue resistance, owing to the introduction of a homogeneous network structure. Finally, the notable synergy resulting from the interplay between the homogenous network structure and the globular protein characteristics of LZM, leading to a considerable reduction in swelling. The LP hydrogel sealant with a homogeneous network exhibits considerable promise for clinical applications in wet, dynamic and concealed wounds such as porcine cardiac hemorrhage, lung leakage, and rat oral ulcers, as depicted in Scheme 1(c). We conducted a series of in vitro and in vivo experiments to demonstrate that the sprayable LZM/4-arm-PEG hydrogel, with a homogeneous network, effectively seals leaks and promotes wound healing, surpassing commonly used clinical agents. It emerges as a promising solution for rapidly addressing wet, dynamic, view-restricted or invisible wound closures within clinical therapy.

2. Experimental section

2.1. Materials

4-arm Poly (ethylene glycol) succinimidyl succinate (4-arm-PEG-NHS), Mw = 10k/20k/40k Da, Mw/Mn = 1.03) was ordered from SINOPEG. Lysozyme protein (LZM) was purchased from Beijing Solabao Technology Co. Sodium tetraborate (AR), and borax (AR), were purchased from Shanghai Ling Feng Chemical Reagent Co. Artificial saliva (Bofimec) was purchased from Shanghai Genesis Technology Co. Mundheil gel® (SOS) was purchased from WINDSTARSOS, Germany. All reagents were of analytical grade and used directly without further purification.

2.2. Hydrogel preparation

Before preparing hydrogel, the LZM was purified through a dialysis-lyophilization process (3 days), and then Borax buffer solutions (20 mg/mL) of different pH values were achieved by adjusting the amounts of boric acid and borax. Next, the prepared borax buffer solution was used as the solvent to dissolve LZM (15 %, w/v) as the precursor A. At the same time, the PBS (1x) was used to dissolve 4-arm-PEG-NHS of different molecular weights (15 %, 10k/20k/40k, w/v) as the precursor B. Finally, the LP hydrogels with different gelation times can be formed in situ after mixing the two components with a double-cylinder syringe (A: B = 1:1, v/v). Precursor B of LZM/2-arm-PEG-2k+20k hydrogel consisted of 2-arm-PEG–NHS–2k (1.66 %, w/v) and 2-arm-PEG–NHS–20k (13.4 %, w/v) dissolved in PBS. LZM/4-arm-PEG–NHS–20k/PBS (LP-20k/PBS) was prepared by lysozyme and 4-arm-PEG–NHS–20k dissolved in PBS.

2.3. Fourier transform infrared spectrum (FTIR) analysis

To study the gelation mechanism of hydrogels, Fourier transform infrared (FTIR) spectra of the pure 4-arm-PEG–NHS–20k powder were used as the control sample were obtained using a TENSOR-27 spectrometer (Bruker, German) scanned in the frequency range of 4000–400 cm^{-1} after the progress of the potassium bromide tableting.

The LP-20k hydrogel was made into a film by freeze-drying. Then Fourier-transform infrared spectrum of LP-20k hydrogel films was obtained on a Thermo Nicolet iS50 spectrometer with attenuated total reflection (ATR) attachment.

2.4. Measurement of gelation time

In this experiment, the gelation time was measured using the vial tilting method. Briefly, at room temperature (25 °C), gelling precursor A and gelling precursor B were prepared in a double-barrel syringe according to the method described above, and the liquid in the syringe was injected into the vial immediately after the start of the timing, and the timing was stopped when it was observed that the liquid in the vial could not flow, and the time recorded was regarded as the gelation time of the group.

2.5. Rheological properties analysis

The hydrogels were prepared as disc-shaped samples with a diameter of 20 mm. The viscoelastic behaviors of the hydrogels were measured by a Thermo Haake MARS rheometer. Before the tests, an amplitude sweep was first performed to define the linear viscoelastic region (LVR) in which the storage modulus is independent of the strain amplitude. Oscillation frequency sweep tests from 0 Hz to 10 Hz were selected to perform the rheological studies. The storage modulus G′ represents the elastic property of the hydrogel, and the loss modulus G″ represents the viscous properties. Time sweep oscillatory tests were performed at 10 % strain (CD mode) and 1 Hz with a 0.5-mm gap. The gel point was determined as the time when the storage modulus (G′) surpassed the loss modulus (G″) [54].

2.6. In vitro testing of the ability of the sprayable LP-20k hydrogel to seal notches and withstand flushing

The LP-20k hydrogel was sprayed on pig skin that had been intentionally notched to evaluate its capacity to seal the notches with 4 mm width. The hydrogel was also sprayed on a moist heart surface and rinsed with high-pressure water to observe the adhesion of the hydrogel.

2.7. Small-angle X-ray scattering (SASX) test

Small-angle X-ray scattering (SAXS) patterns were collected on small-angle X-ray scatterer NanoStar SAXS (Bruker AXS, German) with sample-detector-distance calibration before the measurements. The wavelength of the X-ray irradiation is 0.1542 nm. SAXS patterns were collected with identical exposure times of 300 s for all samples.

The d spacing (a characteristic distance between LZM) was calculated using the following equation $d = 2\pi/Q$, where Q is the peak position at the highest scattering intensity.

2.8. Swelling properties test

To characterize the swelling behavior, the as-prepared hydrogels were immersed in PBS (pH = 7.4) for 24 h on a constant temperature shaker (37 °C, 80 rpm). We determined the weight of the initial sample (W0) and the weight of the sample after swelling (W1), which allowed us to calculate the swelling ratio as follows: Swelling ratio (%) = (W1–W0)/W0 × 100 %. (n = 4).

2.9. Tensile performance test

Hydrogels were prepared as dumbbell-shaped samples (5 × 16 × 2 mm), then stretched at a speed of 10 mm/min until fracture using an ElectroForce® tester (Load Frame 3200 System, BOSE, American) after clamping the samples, and the stress-strain curves were recorded for each sample. For cyclic stretching, the number of machine cycles and the strain of stretching were further set (50 cycles with 100 % strain) (n = 5).

2.10. Compressive performance test

Hydrogels were shaped into cylinders with a height of 6 mm and a base diameter of 10 mm. Then compressed at a speed of 10 mm/min until fracture using an ElectroForce® tester (Load Frame 3200 System, BOSE, American), and the stress-strain curves were recorded for each sample. For cyclic compressing, the number of machine cycles and the strain of compressing were further set (50 cycles with 80 % strain) (n = 5).

2.11. Wet adhesion strength test

To evaluate the bioadhesive performance of the hydrogels, the lap shear tensile stress test was performed according to the procedure of ASTM standard (F2255-05). Briefly, the pig skin was cut into a regular 10 × 20 mm rectangle and immersed in PBS before use. The hydrogels were sprayed between two pieces of pig skin for adhesion.

The skin was then rapidly adhered to the hydrogel to achieve an overlapping area of approximately 10 mm × 10 mm. Methylene blue was added to the prepolymer solution as an indicator to observe the hydrogel residue on the skin surface interface after interfacial separation.

The samples were tested using an Instron mechanical tester at a constant extraction rate of 5 mm/min after 0 h and 24 h of immersion in PBS, respectively (n = 4).

2.12. Adhesion performance in dynamic wet environments

To evaluate the adhesion capacity of LP hydrogels against shear forces in a wet environment. The hydrogel was the formation on the surface of pig skin, then the hydrogel was submerged in water, and the hydrogel was bent 180° and experienced 2000 cycles of underwater shearing at a frequency of 5 times/second to simulate the situation of the hydrogel being flushed and sheared by the body fluids in vivo and being squeezed by external forces. Commercial mouth ulcer gel (Mund-heil gel) was selected as the control group.

2.13. Retention time testing in dynamic wet environments

To evaluate the mechanical and adhesion capacity of LP hydrogels against shear forces in a wet environment. First, the rats were anesthetized with pentobarbital sodium (1 %, 40 mg/kg). The hydrogel formed on the oral mucosa, and the rats were temporarily anesthetized with isoflurane every 30 min to observe hydrogel and record retention time. Commercial mouth ulcer gel (Mund-heil gel) was selected as the positive control group.

2.14. Degradation properties test

The biodegradation behavior of hydrogels was evaluated in a wet state after the hydrogels reached swelling equilibrium. In brief, the hydrogels were placed in a sealed tube containing PBS (pH = 7.4) at 37 °C to simulate the wet environment inside the body. The hydrogels were removed at regular intervals and their mass was recorded after wiping the PBS with filter paper and lyophilization, and the above process was repeated till the hydrogels were completely biodegraded. Finally, the biodegradation ratios of the hydrogels were calculated according to the remaining weight of the hydrogel. The biodegradation ratio was calculated using the following formula:

$$\text{Weight remain ratio} = \text{Wt}/\text{Wb} * 100\% \ (\text{n} = 4)$$

where Wt denotes the weight of the hydrogel following biodegradation for a specific time, and Wb denotes the weight of the initial hydrogel after freeze-drying.

2.15. Bursting pressure test

Bursting pressure test was measured according to previous methods described by Azuma et al. [55]. The pig intestines were used in this experiment. The intestines were linked to a syringe pump and filled with PBS solution. A 1.67-mm hole was created on the intestine surface, and then the hydrogel was formed in situ on the puncture site. The bursting pressure was measured 10 min after the forming of the hydrogel. The pressure at which it began to decrease was considered as the bursting pressure. (n = 3).

2.16. Cytocompatibility testing

To study the cell affinity of the LP-20k hydrogel, murine-derived L929 fibroblast and Human Umbilical Vein Endothelial Cells (HUVEC) cells purchased from the American Type Culture Collection (ATCC, VA, USA) were used for evaluating the cytocompatibility of hydrogel. Cells were incubated in Dulbecco's modified Eagle medium (DMEM, Gibco) supplemented with 10 % fetal bovine serum (Gibco) at 37 °C and 5 % CO_2 in a humidified incubator. Cell proliferation and viability of LP-20k hydrogel were assessed using CCK-8 (Beyotime, China) and Calcein-AM/PI staining kits (Dojindo, Japan), respectively. First, 0.5 mL of precast hydrogel samples were soaked in 3 mL of medium at 37 °C for 24 h. The soaked medium was then aspirated and subsequently sterilized through a 0.22 μm filter to obtain a conditioned medium.

For cell proliferation, L929 cells were inoculated into 48-well plates at a density of 3×10^4 cells per well after adding conditioned medium and cultured for 3 days. Cells cultured in a blank medium were used as a control group. Fresh medium containing 10 % CCK-8 reagent was added to the plates for 120 min at 1,2,3 day. Then, the OD of the solution at 450 nm was recorded to calculate cell proliferation.

$$\text{Cellproliferation}(\%) = (\text{AH-AC})/\text{AC}(\text{n} = 3) \qquad \text{Equation 1}$$

In this equation, AH and AC correspond to the absorbance values of the hydrogel group and control group, respectively.

Meanwhile, the Cell viability of the gel was assessed with L929 cells cocultured with different hydrogel extracts using a Calcein AM/PI Double Stain Kit (MKBio, Shanghai, MX3012) following the manufacturer's protocols. After the preparation of the assay buffer and stain buffer, cells were incubated with the stain buffer at 37 °C for 15 min. Fluorescent images were captured on a confocal microscope (Leica, DMi8) and live and dead cells were counted by Image J.

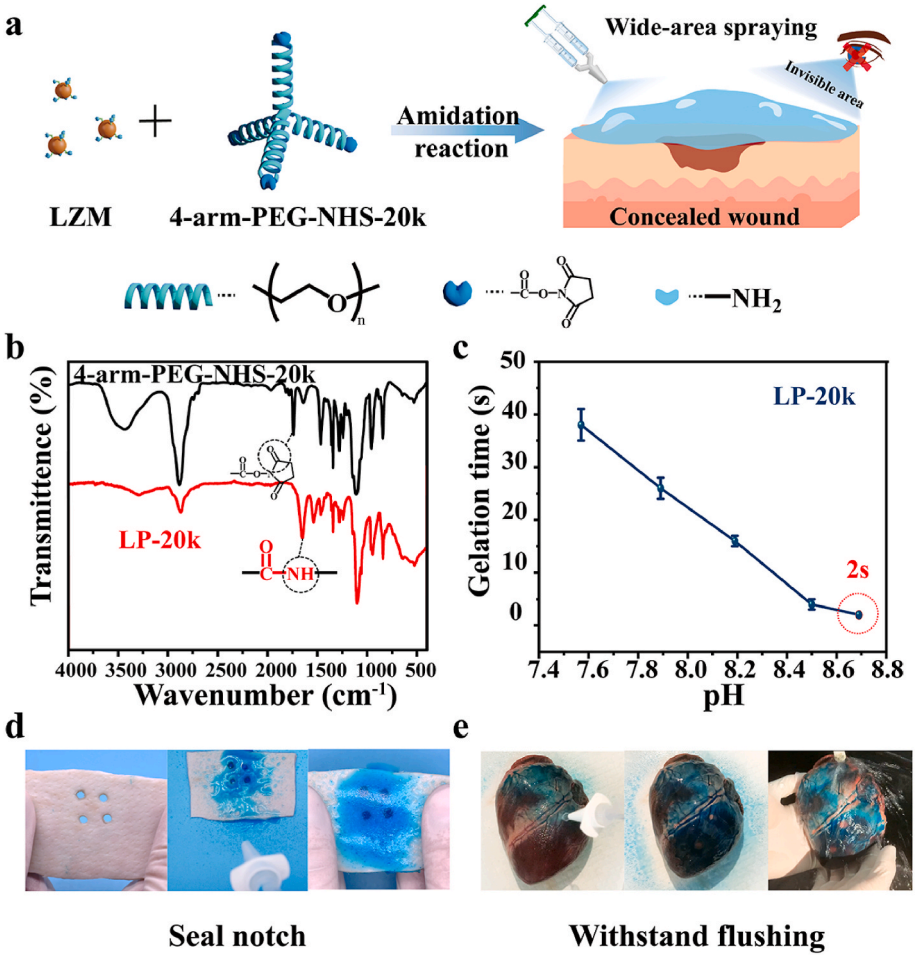

Fig. 1. Preparation and characterization of sprayable LZM/4-arm-PEG-20k (LP-20k) hydrogel. (a) A hydrogel sealant is prepared through the amidation reaction of the amino group of LZM with a reactive ester derived from 4-arm-PEG–NHS–20k. This hydrogel formulation offers the convenience of application through spraying and is suitable for use on concealed wounds. (b) Infrared spectra of 4-arm-PEG–NHS–20k and LP-20k hydrogel. The appearance of the peak at 1525 cm^{-1} indicates that the hydrogels are cross-linked by amide bonding. (c) Gelation time of LP-20k hydrogel at different pH of borax buffer solution (n = 4). (d) Optical photographs of LP-20k hydrogel uniformly sprayed on the wet pig skin to seal four notches with a diameter of 4 mm. e) Optical photographs of the LP-20k hydrogel was uniformly sprayed over a wide area onto a wet pig heart, and experienced water flushing.

$$\text{Cell viability}\ (\%) = \text{Alive}/(\text{Alive} + \text{Adead})\ (n = 3) \qquad \text{Equation 2}$$

In this equation, Alive and Adead correspond to the number of living and dead cells, respectively.

2.17. Hemolysis test

To verify the compatibility of hydrogel in blood, fresh rabbit blood was used to verify biocompatibility with blood. The blood of the rabbit was centrifuged at 1200 g for 15 min to remove the upper serum. The obtained plasma was washed with PBS buffer (repeated 3 times), then 1 mL rabbit blood cells (40 %, v/v) in PBS buffer (pH 7.4) was incubated with hydrogel (500 μL) for 1 h at 37 °C. At the same time, 500 μL PBS buffer or 0.1 % Triton X-100 solution was added into rabbit blood cell suspension as positive and negative controls, respectively. These tubes were then centrifuged at 1200 g for 15 min and absorbance at 540 nm of supernatant was measured by a microplate reader (SpectraMaxi, Molecular Devices). The ratio of hemolysis for LP-20k hydrogel was calculated as:

$$\text{Hemolysis}(\%) = (\text{Ah-Ap})/(\text{At-Ap}) \times 100\%\ (n = 3) \qquad \text{Equation 3}$$

In this equation, Ah, Ap, and At represent the absorbance of the hydrogel group, positive group (PBS), and negative group (Triton X), respectively.

2.18. Antimicrobial performance test

Staphylococcus aureus (*S. aureus*, ATCC 25923, acquired from the Second Affiliated Hospital of Zhejiang University) was chosen as the model of Gram-positive bacteria, and *Escherichia coli* (*E. coli*, ATCC 25922, acquired from the Second Affiliated Hospital of Zhejiang University) was chosen as the model of Gram-negative bacteria.

First, the bacteria were incubated in a liquid medium at 37 °C and shaken overnight at 80 rpm. Before use, the bacteria were centrifuged and resuspended in the liquid medium. Then, 1 mL of bacterial suspension (1×10^7 CFU/mL^{-1}) was added to the surface of 2 mL of hydrogel. And set the 0.9 % saline group was considered the control group. After incubation at 37 °C for 12 h, the culture solution was blown and resuspended. Its turbidity was tested at 600 nm to obtain the bacterial viability, which was calculated as follows:

Bacterial viability (%) = (OD of bacterial suspension in saline - OD of bacterial suspension on the surface of hydrogel)/(OD of bacterial suspension in saline) × 100 % (n = 3).

The resuspended bacterial suspension was transferred to a sterilized tube, a series of dilutions were performed with saline, and 100 μL of the bacterial suspension was spread on an agar plate.

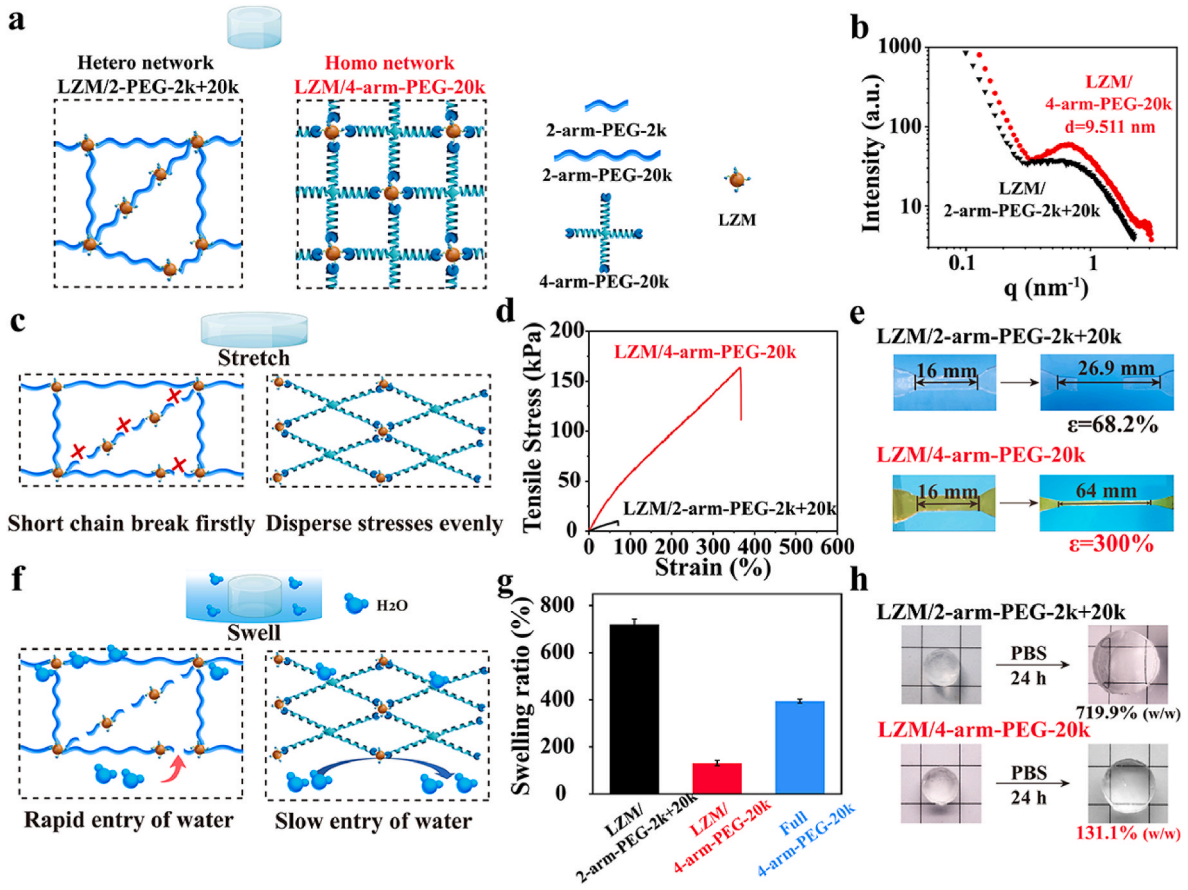

Fig. 2. Validation of LZM/4-arm-PEG-20k hydrogel homogeneity and its impact on the mechanical and swelling properties. (a) Schematic diagram of the network structure and composition of heterogeneous network hydrogel (LZM/2-arm-PEG-2k+20k) and homogeneous network hydrogel (LZM/4-arm-PEG-20k). (b) SAXS profiles of hydrogels of LZM/2-arm-PEG-2k+20k and LZM/4-arm-PEG-20k. (c) Schematic representation of when the hydrogel is stretched, the short chain breakage in the LZM/2-arm-PEG-2k+20k, and the molecular chains being uniformly stretched in the LZM/4-arm-PEG-20k. (d) Tensile stress-strain curves and (e) optical photographs of LZM/2-arm-PEG-2k+20k and LZM/4-arm-PEG-20k being stretched to different degrees. (f) Schematic representation of disruption of heterogeneous network structure leads to rapid entry of water and intact, the homogeneous network structure restricts water entry during swelling. (g) Swelling ratios of the LZM/2-arm-PEG-2k+20k and LZM/4-arm-PEG-20k and full 4-arm-PEG-20k after being submerged in PBS for 24 h, and (h) optical images of the hydrogel before and after swelling (*$p < 0.05$, **$p < 0.01$ and ***$p < 0.001$; $n = 4$).

2.19. Heart hemorrhage and lung leakage in pigs

In vivo studies were performed in strict accordance with National Institutes of Health (NIH) guidelines for the care and use of laboratory animals (NIH Publication no. 85-23 Rev. 1985) and all procedures were approved by the Research Center for Laboratory Animals of Shanghai University of Traditional Chinese Medicine (Shanghai, China). To test the ability of LP-20k hydrogel to seal wet dynamic wounds, we take the extreme heart bleeding model and the lung-blowing model in pigs (white pig, 60 kg). In the pig heart bleeding model, the pigs were first anesthetized with pentobarbital sodium (3 %, 40 mg/kg) to perforate the porcine heart with a punch with a diameter of 6 mm. Then the LP-20k hydrogel was directly applied to observe the sealing condition without the aid of a suture bag. Fibrin glue was selected as the positive control group. Observe hydrogel retention after two weeks.

In the model of air leakage in the lung, first, use a scalpel to draw a 30 mm wide and 10 mm deep wound in the lung, then reduce the tidal volume to 250 mL, spray LP-20k hydrogel, and gradually increase the tidal volume (250 mL each time), hold for 1 min at each tidal volume, inject the liquid with physiological saline to assist in observing whether there is air leakage.

2.20. The therapeutic effect on oral ulcers in rats

To further test the ability of LP-20k hydrogel to seal wounds and promote healing, SD rats (male, age eight weeks, 250 g ± 10 g) were used for the experiments and were anesthetized intraperitoneally with sodium pentobarbital (1 %, 40 mg/kg). The formation of oral ulcers was first induced by placing circular filter paper (5*5 mm) soaked in 70 % acetic acid solution for 3 min in the buccal membrane of the mouth. Then, we compared the therapeutic effect of a commercial ulcer gel (Mund-heil gel) with LP-20k. On the second day after the induction of oral ulcer formation (day 0), LP-20k hydrogel and Mund-heil gel were applied to the oral ulcers, and rats without treatment were set as the control group ($n = 5$). The retention of the material was observed at 30 min, 1 h, 3 h, 6 h, 9 h, and 12 h after application, and wound healing was observed on days 1, 3, 5, and 7. Animals were sacrificed on days 1 and 7 after application of the material. Samples of the oral mucosa from the ulcer were collected for paraffin sectioning and analyzed histologically and immunohistochemically (HE staining), and the inflammatory response was assessed with antibody CD-11b.)

2.21. Statistical analysis

All data were expressed with mean standard deviation (SD) and analyzed using one-way ANOVA with post hoc tests. Significance was set at $p < 0.05$ (***$p < 0.001$, **$p < 0.01$, *$p < 0.05$), while $p > 0.05$ was considered to be statistically nonsignificant (N.S.).

3. Results and discussion

3.1. Fabrication and characterization of PEG-LZM sprayable hydrogel

A facile one-step strategy was employed to prepare PEG-LZM sprayable hydrogels. Specifically, a dual-syringe sprayer was employed for the mixing and application of lysozyme (LZM) and 4-arm-PEG-NHS (Mw = 20 kDa) precursors. Within this procedure, the amino groups of LZM engaged in an amidation reaction with the active esters of 4-arm-PEG–NHS–20k, leading to in situ gelation directly on the wound (Fig. 1 (a-b)). The resultant hydrogel is designated as LZM/4-arm-PEG-20k (LP-20k). Thanks to the reaction can be gently conducted at room temperature without causing harm to the tissue, the resultant LP-20k hydrogel is envisaged for in situ application in clinical wound sealing [56,57]. To ensure the rapid solidification of the hydrogel in situ, the content of the PEG was adjusted to expedite gelation. As shown in Figure S1, when the solid content of PEG was increased from 5 % to 15 % (w/v) and the pH value of the borax buffer solution was kept at 8.12, the gelation time progressively shortened. This outcome aligns with expectations, as higher polymer concentrations facilitate and expedite the cross-linking reaction. It is worth noting that further increasing the content of 4-arm-PEG–NHS–20k beyond 20 % (w/v) may cause challenges in dissolving PEG and cause entanglements between polymer chains, deteriorating chain mobility and subsequently slowing down gelation process [58]. Therefore, we selected a LP-20k hydrogel with a 15 % (w/v) PEG in the subsequent experiments to achieve an appropriate gelation time. Furthermore, as demonstrated in Figure S2 and Figure S3, through the adjustment of the LZM's solid content, we observed that the hydrogel exhibited optimal mechanical performance and resistance to swelling when the LZM's solid content was set at 15 % (w/v). This may be attributed to the hydrogel possessing an appropriate cross-linking density at this particular ratio. Additionally, given that the amidation reaction is nucleophilic, the pH of the borax buffer solution for gelation is adjusted to promote the deprotonation of amine groups on LZM to expedite the reaction [59]. In brief, this was accomplished by adjusting the borax content in the borax buffer solution. It's worth noting that gelation occurs in approximately 2 s when the pH of the borax buffer solution is set at 8.70 in Fig. 1(c). As depicted in Figure S4, the storage modulus (G′) curve intersects with the loss modulus (G″) curve at 2 s, providing further evidence that the transition from solution to hydrogel occurs within 2 s.

To assess the efficacy of the sprayable LP-20k hydrogel in sealing concealed wounds, a sealing performance test on multiple notches was conducted. Four notches with a diameter of 4 mm were created to simulate the concealed wounds. Visual examination of optical photographs revealed that LP-20k rapidly and simultaneously sealed multiple small notches in Fig. 1 (d) and exhibited the ability to cover extensive and irregular tissue surface of heart and keep adhesion while withstanding flushing in Fig. 1 (e) and Video S1.

To investigate the degradation time required for the in vivo application of sprayable LP-20k hydrogel, its degradation performance was assessed in vitro. As shown in Figure S5, the LP-20k hydrogel was completely degraded in vitro by the seventh day, confirming the material's potential for internal application.

These results show that the LP-20k hydrogel exhibits favorable sprayability and is capable of achieving rapid gelation to effectively seal concealed wounds, even within moist environments.

3.2. Verification of network homogeneity

To investigate the homogeneity of the network structure within LZM/4-arm-PEG-20k hydrogel, two linear PEGs (2-arm-PEG–NHS–2k and 2-arm-PEG–NHS–20k) were employed in the hydrogel formation, simulating the formation of a heterogeneous network structure that typically arises during the conventional cross-linking of polymers in Fig. 2 (a). The number of chemical cross-linking points in the heterogeneous network hydrogel remained consistent with that of the LP-20k hydrogel. These resultant hydrogels were labeled as LZM/2-arm-PEG-2k+20k and LZM/4-arm-PEG-20k, respectively.

Since LZM can be seen as a cross-linking agent in hydrogels, the homogeneity of the hydrogel's network structure was directly verified by using small-angle X-ray scattering (SAXS) to examine the distribution of LZM [60,61]. As depicted in Fig. 2 (b), the LZM/4-arm-PEG-20k hydrogel exhibits a prominent diffraction peak at q = 0.661 nm^{-1}, indicating a periodic arrangement of LZMs within the hydrogel network (d = 9.511 nm). Conversely, the LZM/2-arm-PEG-2k+20k hydrogel does not display any discernible diffraction peaks but a broad plateau, suggesting that the LZMs are disordered and lack a periodic arrangement within the hydrogel system. Moreover, SAXS of the LZM/4-arm-PEG-20k hydrogel from different positions was tested and we found that the SAXS curves almost overlapped, which further demonstrated that the LZM/4-arm-PEG-20k hydrogel exhibits a spatially homogeneous network structure (Figure S6).

We next assess the tensile properties, rheological properties, and swelling ratio of the hydrogels. The results presented in Fig. 2 (d-e) demonstrate that the LZM/4-arm-PEG-20k hydrogel exhibits greater deformation and superior mechanical properties compared with the LZM/2-arm-PEG-2k+20k hydrogel. This phenomenon can be attributed to the fact that during the stretching of hydrogels, a homogeneous network tends to promote an even distribution of stress within all constituent chains, whereas a heterogeneous network leads to premature breakage of the shorter chains [62,63]. Consequently, a hydrogel with a heterogeneous network experiences rupture before those with a homogeneous network.

The rheological testing of LZM/2arm-PEG-2k+20k hydrogel and LZM/4arm-PEG-20k hydrogel provides their respective G' (storage modulus) and G'' (loss modulus) values, which, through the formula $\tan\theta = G''/G'$, reflect the hydrogel's elastic properties. G′ represents the energy stored due to elastic deformation (reversible) during hydrogel deformation, while G″ indicates the magnitude of energy dissipated due to viscous deformation (irreversible). As depicted in Figure S7, the tanθ value of LZM/2arm-PEG-2k+20k hydrogel (0.26066) is significantly higher than that of LZM/4arm-PEG-20k hydrogel (0.01367). This discrepancy can be attributed to the energy consumption during deformation, primarily arising from the presence of dangling chains and entanglement-related network defects [41,64].

Fig. 2 (g-h) indicates that the LZM/2-arm-PEG-2k+20k hydrogel exhibits a considerably higher swelling ratio than the LZM/4-arm-PEG-20k hydrogel in 24 h. The observed outcome can be attributed to the maintenance of stability in the homogeneous network, while the heterogeneous network experiences fracture as it undergoes swelling [42]. Furthermore, the swelling ratio of LZM/4-arm-PEG-20k hydrogel is observed to be lower than that of full 4-arm-PEG-20k hydrogel which was prepared using 4-arm-PEG-NH_2 and 4-arm-PEG-NHS, thereby confirming the structural stability advantages of the LZM.

In conclusion, our results demonstrate the LZM/4-arm-PEG-20k hydrogel, composed of lysozyme with a spherical structure and 4-arm-PEG with an orthotetrahedral structure, has a homogeneous network structure. Additionally, the constructed homogeneous network hydrogels exhibit outstanding stretchability, minimal energy dissipation, and reduced swelling properties in contrast to heterogeneous network hydrogels.

3.3. Mechanical properties of LZM/4-arm-PEG (LP) hydrogels with varying PEG molecular weight

We next evaluate the mechanical properties of homogeneous network hydrogels with different PEG molecular weights. For this study, 4-arm-PEG–NHS–10k/20k/40k with mono-arm PEG Mw at 2.5, 5, and 10k respectively, were selected as the precursors, ensuring uniform mixing with LZM and smooth spraying [37]. The resultant hydrogels are designated as LP-10k, LP-20k and LP-40k, respectively.

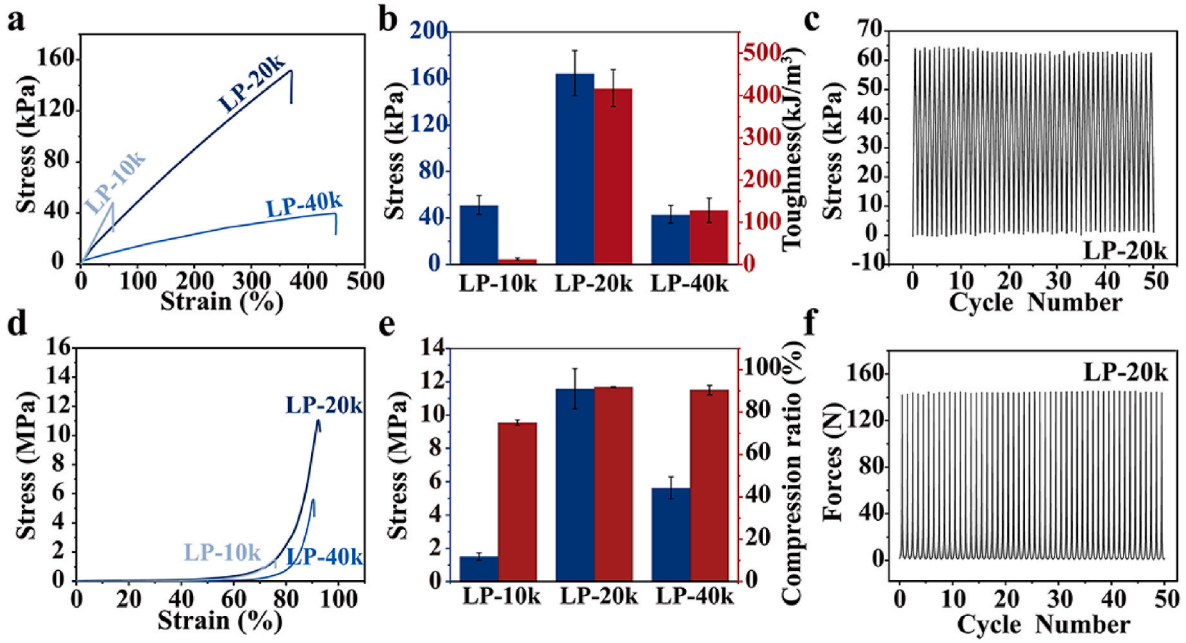

Fig. 3. Mechanical properties of homogeneous network LZM/4-arm-PEG (LP) hydrogels with different molecular weights. (a) Tensile stress-strain curves of LP hydrogels with different molecular weights, and (b) tensile strength and toughness (n = 4). (c) Stress-cycle curve of LP-20k under cyclic tensile loading-unloading for 50 cycles (n = 3). (d) Compressive stress-strain curves of LP hydrogels with different molecular weights, and (e) compressive strength and maximum compressive strain (n = 4). (f) Compressive forces-cycle curve of LP-20k under cyclic compressive loading-unloading for 50 cycles (n = 3).

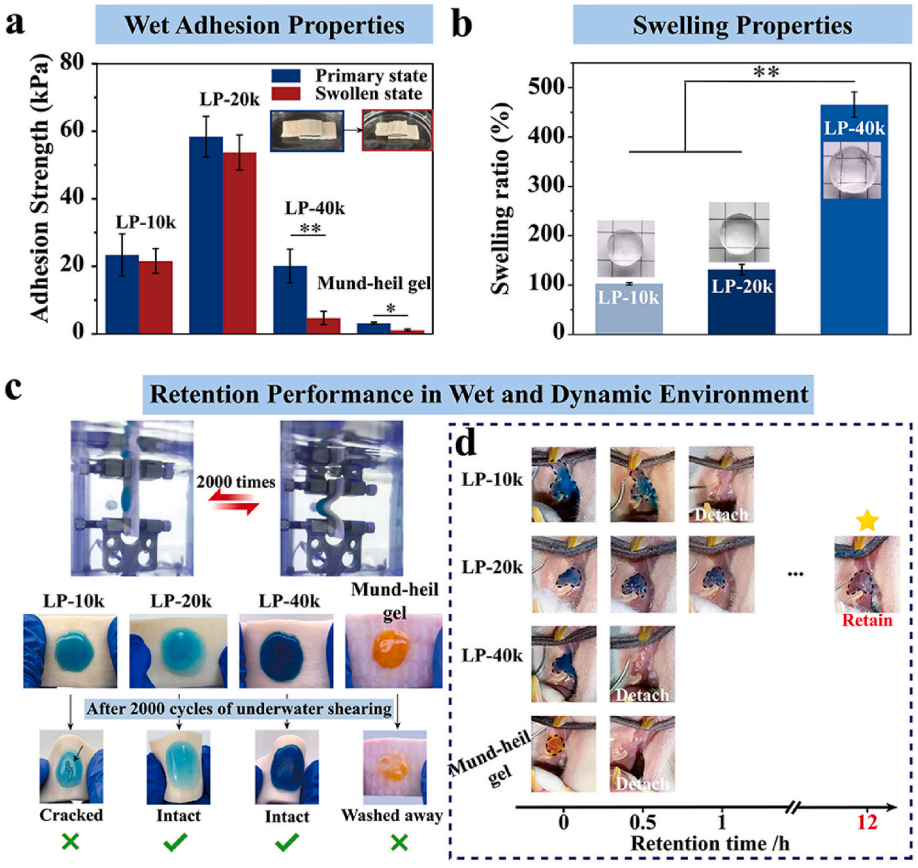

Fig. 4. Wet adhesive and swelling properties of the homogeneous network LP hydrogels at different molecular weights and their retention performance in wet and dynamic environment. (a) The initial adhesive strength and the adhesive strength after swelling for 24 h of LP hydrogels with different molecular weights. (b) Swelling ratio of LP hydrogels with different molecular weights soaked in PBS for 24 h. (c) Retention performance of LP hydrogel with different molecular weights and Mund-heil gel after 2000 cycles of underwater shearing and (d) retention performance in the rat oral cavity (*p < 0.05, **p < 0.01; n = 4).

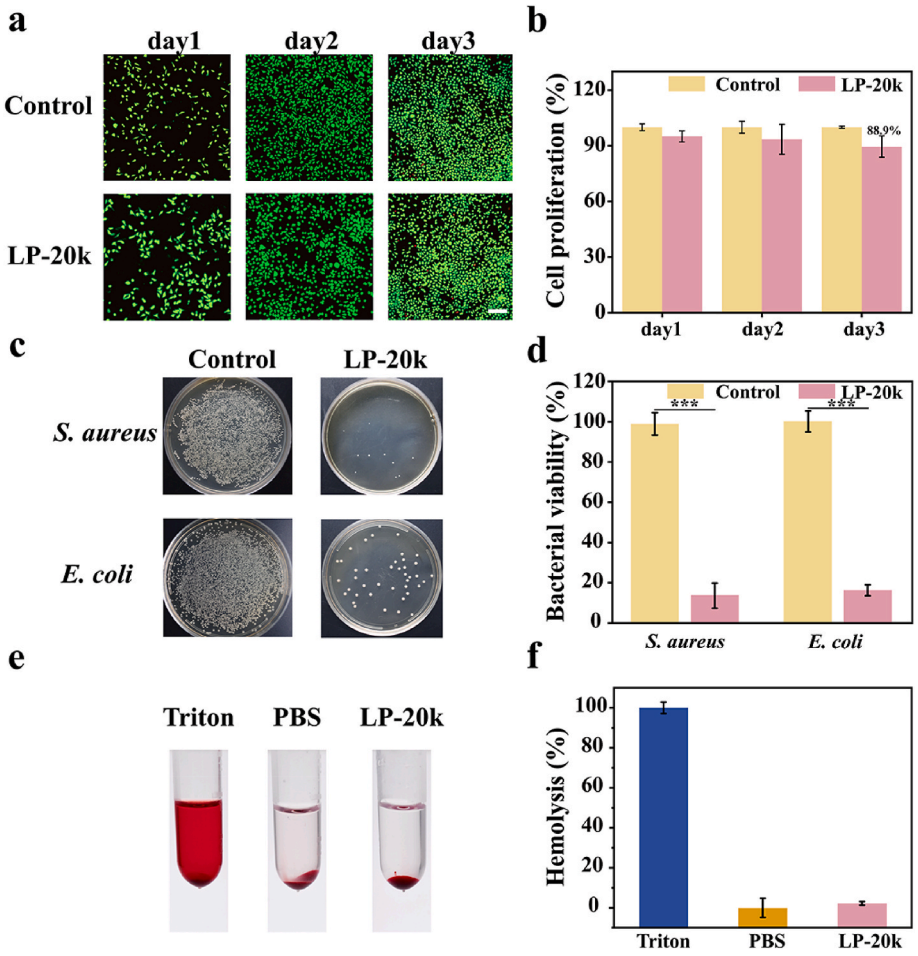

Fig. 5. Biocompatibility and antibacterial properties of LP-20k hydrogel. (a) Live/Dead staining and (b) Cell proliferation of L929 cells after incubating in hydrogel extracts for 1, 2, and 3 d. The group incubated without extract served as the control (Scale bar: 200 μm). (c) Digital photographs of CFUs grown on LB agar plates and (d) quantification of bacterial viability percentages of *S. aureus* and *E. coli* after incubation with LP-20k hydrogel. The group incubated with 0.9 % saline served as the control. (e) Digital photographs showed the results of the hemolysis assay and (f) quantification of hemolysis ratios in each group. Triton indicated Triton X-100 solution (0.1 %) (*$p < 0.05$, **$p < 0.01$ and ***$p < 0.001$; $n = 4$).

Firstly, the homogeneous network characteristics of the three hydrogels were ensured through SAXS. The curves elucidate that LP-10k/20k/40k hydrogels each exhibit pronounced diffraction peaks without plateaus, thus affirming their periodic distribution of LZMs (Figure S8). This phenomenon implies the presence of a homogeneous network structure within these hydrogels. The distances (d) between LZMs increase with the augmentation of molecular weight, potentially attributed to chain elongation resulting in an extended separation between cross-linking points (LZM).

To examine the influence of varying PEG molecular weight on the mechanical properties of the hydrogels, we conducted tensile performance assessments. Notably, it becomes apparent that the extensibility of the hydrogels increases proportionally with higher molecular weights in Fig. 3 (a-b). This observed phenomenon can be ascribed to the enhanced flexibility of polymer chains and their improved capacity to store energy through conformational transitions, specifically transitioning from a coiled to an extended state, as the molecular weight increases. However, it is worth noting that the LP-40k hydrogel, while exhibiting an impressive stretchability of up to 450 %, concurrently demonstrates a comparatively low modulus. This peculiarity can be attributed to the relatively limited presence of chemical crosslinking points within the hydrogel structure, as detailed in Figure S9. The low modulus property, relative to the surrounding tissue, renders the hydrogel susceptible to deformation, thereby potentially leading to secondary wound damage and impeding the natural wound healing process [65]. Furthermore, the LP-20k hydrogel showcases an optimal combination of ultimate stress and toughness among the tested variants.

The mechanical properties of the LP hydrogel through dynamic compression testing were also investigated. It was observed that with increasing molecular weight, the hydrogel displayed an improved capacity to endure higher degrees of compression (up to 90 %), as illustrated in Fig. 3 (d). As evident from Fig. 3 (e), LP-20k hydrogel demonstrated superior compression stress and ratio. Therefore, the LP-20k was selected for cyclic tensile and compressive testing, aimed at evaluating its fatigue resistance.

The hydrogel exhibits remarkable fatigue resistance, maintaining consistent mechanical properties even undergoing 50 repeated cycles of loading and unloading in Fig. 3 (c-f). This phenomenon arises from the absence of an imperfection network within the homogeneous hydrogel structure, preventing energy loss during deformation and recovery [66].

In summary, the aforementioned findings affirm that the LP-20k hydrogel showcases favorable properties, including a modulus that is in accordance with various tissues (80 kPa) [65], significant extensibility (350 %), fatigue resistance that maintains mechanical stability undergoing 50 repeated cycles of loading and unloading, and high toughness (400 kJ/m^3). The hydrogel is well-suited for efficiently sealing dynamic tissue wounds, mitigating adhesion failure resulting from mechanical mismatch.

3.4. Wet adhesion, swelling and retention performance of LZM/4-arm-PEG (LP) hydrogels with varying PEG molecular weight

To investigate the influence of varying PEG molecular weights on the wet adhesion properties of LP hydrogels, a procedure involving the immersion of hydrogels in PBS for 24 h to induce swelling was carried out, followed by subsequent testing of adhesive strength. A commercially available Mund-heil gel which is mainly composed of hyaluronic acid was used as a control. As depicted in Fig. 4 (a), it becomes evident that the LP-20k hydrogel exhibits notably robust adhesion strength, surpassing that of both LP-10k, LP-40k, and Mund-heil gel. Moreover, as depicted in Figure S10, the burst pressure of LP-20k is significantly superior to that of LP-10k and LP-40k hydrogels. The adhesive strength can be attributed to the bond energy that establishes a connection between the hydrogel and the tissue, as well as the internal cohesion of the hydrogel [67]. Therefore, the exceptional adhesive performance of LP-20k can be attributed to its heightened cohesion, which is linked to its mechanical characteristics when compared to the LP-10k and LP-40k hydrogels. In contrast to previous methods that relied on phenolic hydroxyl groups for wet adhesion through hydrogen bonding, this hydrogel uses a rapid covalent reaction between NHS of PEG and NH_2 of tissue, effectively reducing the influence of the hydration layer on hydrogel adhesion performance, while also enhancing the hydrogel's stable adhesion in wet environments [68–70].

Furthermore, it is noteworthy that the adhesive strength of both LP-10k and LP-20k hydrogels experiences relatively minor changes during the swelling process, whereas that of the LP-40k hydrogels demonstrates a substantial decrease.

Fig. 4 (b) exhibits that LP-10k and LP-20k hydrogels manifest a lower swelling ratio in contrast to LP-40k hydrogel. The high swelling of LP-40k may be attributed to as the molecular weight increases, the content of active esters decreases resulting in a lower cross-linking density in the hydrogel. Interestingly, a correlation emerges between the variations in swelling ratio and changes in adhesive strength. This implies that the slight reduction in adhesive strength observed in LP-10k and LP-20k hydrogels may be attributed to their lower swelling ratios, which contribute to the maintenance of their internal structure. Conversely, the higher swelling ratio observed in LP-40k hydrogels leads to internal structural impairment, consequently diminishing adhesive strength.

To assess the ability of wound closure retention under repeated external shear forces, LP gels were initially applied to the surface of pig skin and exposed to water shearing induced by deformation of the pig skin. The retention status was closely monitored, as documented in **Video S2**. As a positive control, Mund-heil gel was used for comparison. As illustrated in Fig. 4 (c), after enduring 2000 cycles of underwater shearing, cracks became apparent in the LP-10k hydrogel, and the Mund-heil gel was washed away. In contrast, both the LP-20k and LP-40k hydrogels remained structurally intact, exhibiting resilience against the shearing forces. This outcome can be attributed to the remarkable ductility and adhesive properties possessed by these hydrogels.

Furthermore, an assessment of the hydrogels' adhesive properties on the dynamic and moist oral mucosa in vivo was conducted [54,71]. Fig. 4 (d) shows that the LP-10k hydrogel, LP-40k hydrogel, and the commercial Mund-heil gel experienced detachment within 1 h. This outcome is likely attributed to their inadequate adhesion performance when subjected to mucosal deformation and salivary flushing. In contrast, the LP-20k hydrogel remained tightly adhered to the oral

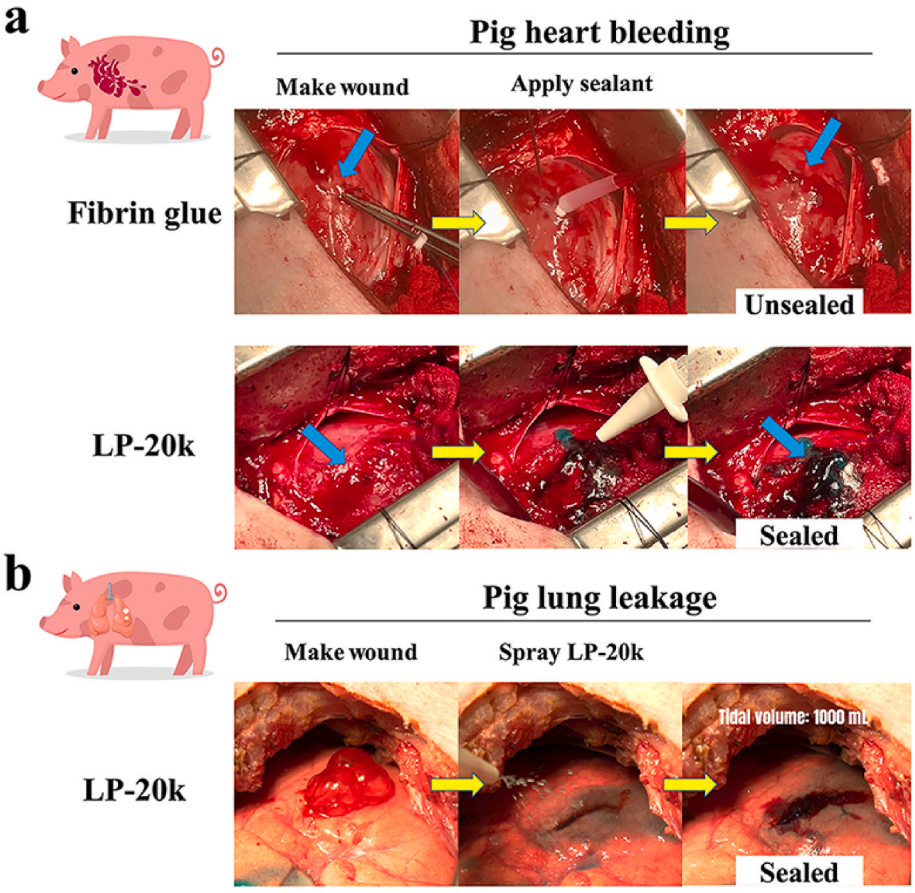

Fig. 6. Sealing performance of LP-20k hydrogel in wet dynamic wound in pigs. (a) Pig heart puncture (6 mm) hemorrhage model, a series of photos demonstrating the ineffectiveness of fibrin glue in wound sealing, contrasted with the rapid wound-sealing capability of LP-20k (the blue arrow points to the wounds). (b) Pig lung large incision wound (3 cm width, 1 cm depth) model, a series of photos illustrating the rapid wound-sealing capability of LP-20k.

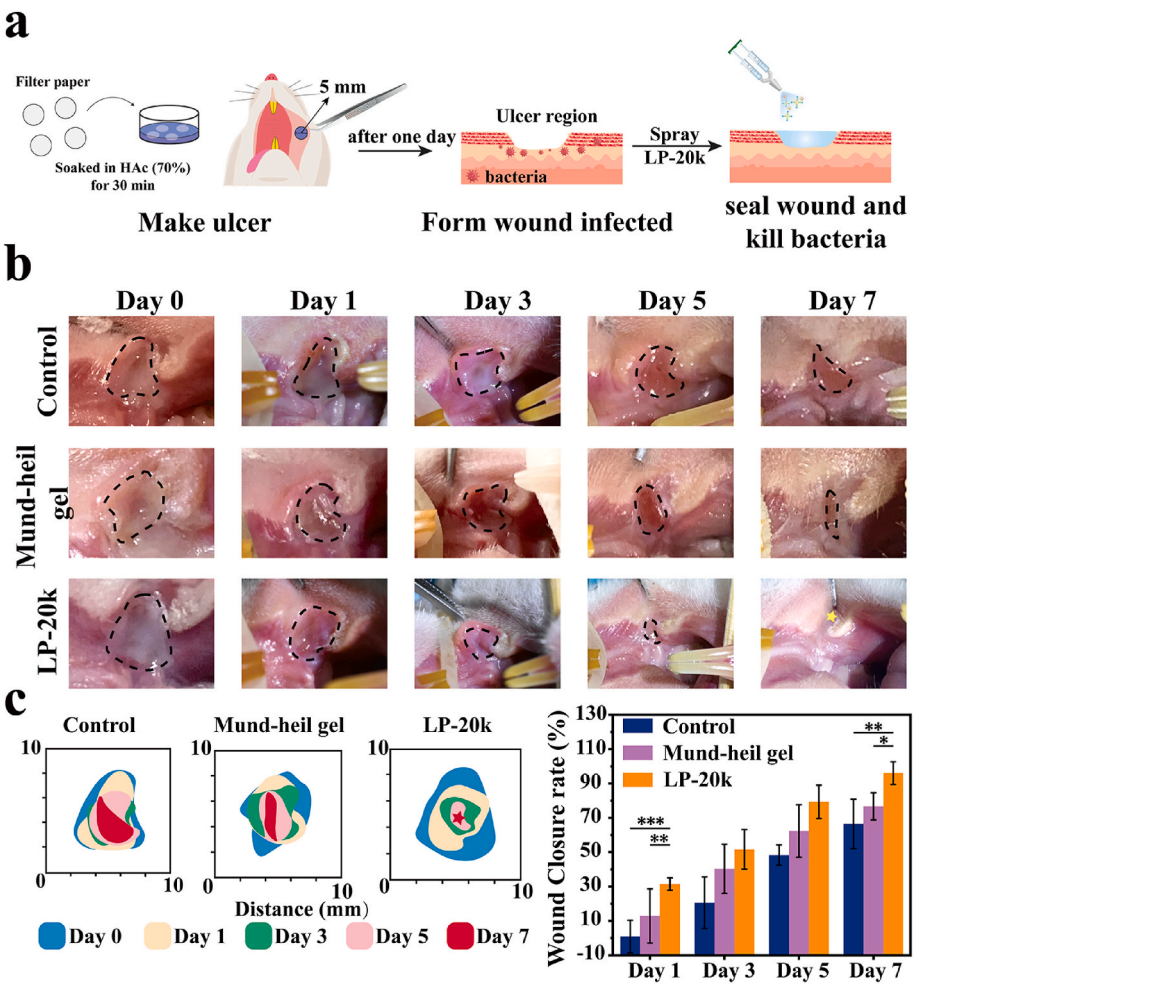

Fig. 7. Therapeutic efficacy of different gels in oral ulcers. (a) The schematic diagram illustrated the surgery to create oral ulcers in rat oral mucosa by acetic acid (70 %) patch. And the process of spraying LP-20k to seal oral wounds and kill bacteria. (b) Gross images of oral ulcers wound treated without treatment (control), with the commercially available Mund-heil gel, with LP-20k at days 0, 1, 3, 5, and 7. (c) Analysis of wound healing traces on days 0, 1, 3, 5 and 7. And quantitative analysis of the wound closure rate of the control, Mund-heil gel, and LP-20k groups (*$P < 0.05$; **$p < 0.01$ and ***$p < 0.001$; $n = 4$).

mucosa even after 12 h.

In conclusion, the LP-20k hydrogel sealants exhibit superior efficacy in sealing wet and dynamic wounds. Consequently, the LP-20k hydrogel was selected for subsequent investigations concerning its closure efficacy and biological impacts in the ensuing experiments.

3.5. Biocompatibility and antimicrobial properties

The biocompatibility of the hydrogel sealants is evaluated, in this study, Mouse fibroblasts (L929) were used to assess the cytotoxicity of the hydrogel by staining the fluorescence of live and dead cells (Fig. 5 a). The results indicate that both the hydrogel group and the control group have a low count of dead cells, with a small difference in cell survival rates between them in Figure S11. Evident from the fluorescence images is the substantial cell proliferation observed over a three-day interval. Subsequently, the quantitative data of L929 cell proliferation was obtained by using the cell counting kit-8 (CCK-8). The results indicate that by the third day, the proliferation rate in the hydrogel group (88.9 ± 5.7 %) was comparable with that in the control group (100 ± 0.517 %) in Fig. 5 (b). This discovery implies that the borax buffer solution demonstrated negligible cytotoxicity, thus affirming the favorable cytocompatibility of the LP-20k hydrogel. Furthermore, we conducted cell compatibility testing of the hydrogel using endothelial cells (HUVEC). As evident from Figure S12, the experimental results align with those from L929, demonstrating no significant cytotoxicity.

Hydrogels were subcutaneously implanted to assess their biocompatibility in vivo. As depicted in Figure S13, on the seventh day after implantation, there were notably few inflammatory cells around the hydrogel, indicating that subcutaneous implantation of LP-20k hydrogel elicited a mild host inflammatory response. This evidence underscores the excellent biocompatibility of the hydrogel.

Antimicrobial hydrogels are highly recommended for wound healing, given that bacterial infections frequently contribute to substantial delays in the healing process [72,73]. To evaluate the antimicrobial properties of hydrogels, Gram-positive *Staphylococcus aureus* (*S. aureus*) and Gram-negative *Escherichia coli* (*E. coli*) were employed as bacterial models and co-cultivation of bacterial fluid with the hydrogels for 18 h. The results revealed substantial antimicrobial bioactivity of the LP-20k hydrogel against both bacteria in Fig. 5 (c-d). To investigate the source of the antimicrobial effect, we also tested the antimicrobial properties of LZM/4-arm-PEG–NHS–20k/PBS (LP-20k/PBS) hydrogel and borax buffer solution. As depicted in Figure S14, LP-20k/PBS hydrogel showed no significant antimicrobial effect, while the borax buffer solution exhibited antimicrobial properties. Hence, we can infer that the hydrogel's antimicrobial effect is derived from the borax buffer solution.

Given that bleeding frequently occurs before visualizing the wound, it is imperative for wound closure materials to have minimal or no hemolytic effects when exposed to blood. Both the LP-20k hydrogel and the PBS supernatant exhibited clarity and demonstrated minimal hemolysis (2 ± 0.91 %) in Fig. 5 (e-f).

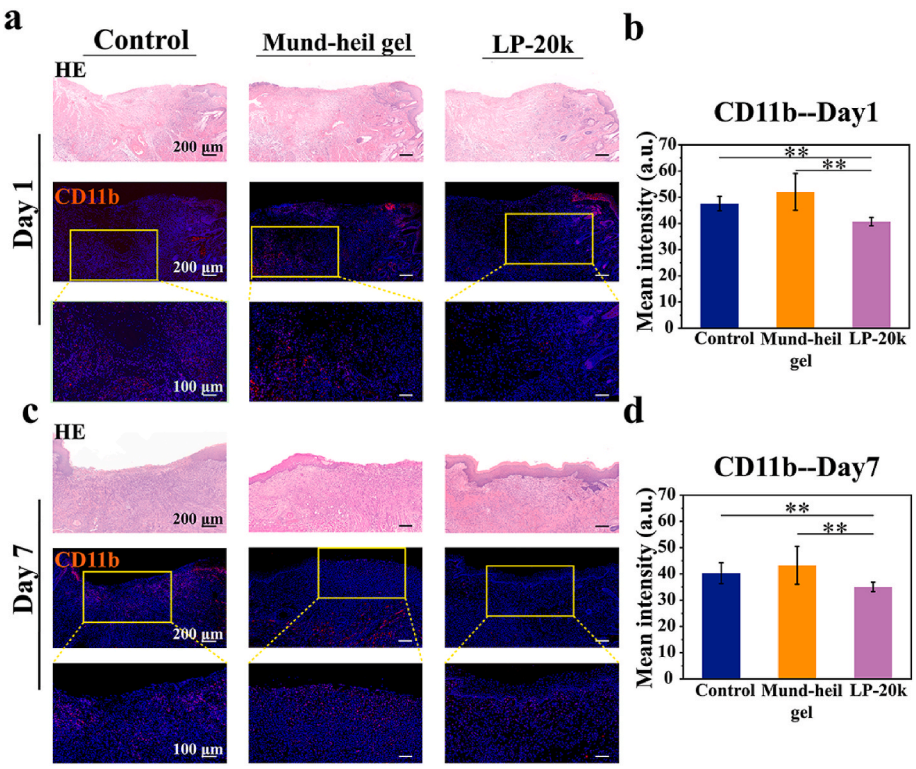

Fig. 8. H&E staining and immunohistochemical staining with CD11b polyclonal antibody (CD11*b*, red) of rat buccal mucosa tissue undergoing different treatments at (a) day 1 and (b) day 7. Quantification of the mean fluorescence intensity of different treatments from fluorescence images at (c) day 1 and (d) day 7. Nuclei (blue) were stained with DAPI (*P < 0.05; **p < 0.01 and ***p < 0.001; n = 3).

3.6. Sealing capabilities in wet dynamic wounds models (heart bleeding, lung leakage) in pigs

To evaluate the efficacy of the LP-20k hydrogel in sealing concealed wounds under dynamic and wet conditions, a comprehensive range of wet wound closure models was strategically employed, encompassing pig heart bleeding to simulate heightened blood pressure and lung leakage to simulate elevated air pressure.

For the experiments involving pig heart bleeding, a female white pig with a weight of 60 kg was initially anesthetized using sodium pentobarbital. Subsequently, a thoracotomy was performed while the pig was in a supine position, aided by isoflurane anesthesia delivered through the bronchus. In the porcine heart bleeding model, a 6 mm puncture was created in the left ventricle of the heart, leading to an immediate release of blood under high pressure. During the surgical procedure, as depicted in Figure S15, a drainage tube was used to eliminate any leaked gel solution promptly to prevent tissue adhesion. Following the puncture, both fibrin glue and LP-20k hydrogel were applied in Fig. 6 (a). Notably, **Video S3** exhibited rapid and successful sealing of the wound by the LP-20k hydrogel, even in the presence of high-pressure bleeding conditions. In contrast, the conventional surgical sealant fibrin glue failed to seal, even when assisted by a stitching bag (**Video S4**). Additionally, the LP-20k hydrogel demonstrated sustained adherence to the heart's surface and underwent partial degradation over two weeks (Figure S16). Over the two weeks, we monitored the cardiac function of the pig using ultrasound. As depicted in Figure S17, Ejection Fractions (EF) and Fraction Shorting (FS) of the pig cardiac remained within the normal range, showing no significant changes compared to pre-experiment levels. This observation provides evidence that the LP-20k hydrogel exhibits effective and sustainable hemostatic effects without generating any adverse effects.

In the lung leakage model, an incision measuring 3 cm in length and 1 cm in depth was made in the lung, leading to the release of gas from the incision. Following this, the LP-20k hydrogel was applied to the wound in Fig. 6 (b). **Video S5** provides clear evidence of the hydrogel's ability to swiftly close the incision within a mere 5 s. Moreover, the LP-20k hydrogel consistently and effectively sealed the incision even under conditions of significant lung deformation and high pressure (the tidal volume was increased to 1000 mL).

In summary, the successful closure achieved in the above-described wounds implies that achieving closure for concealed wounds should be attainable.

3.7. Therapeutic efficacy in concealed wounds model (oral ulcers)

To further investigate the capability of LP-20k hydrogel in sealing dynamic, wet and concealed wounds and enhancing wound healing, oral ulcers were induced using patches soaked in acetic acid (70 %) and LP-20k hydrogel was applied to the wound. Mund-heil gel, a commercially available product commonly used in the treatment of oral ulcers, was used as a positive control in Fig. 7 (a).

The rats were observed to monitor the progression of wound healing on days 1, 3, 5 and 7 after brief anesthesia. It is evident that the wound area in all groups gradually decreased and LP-20k displayed the fastest rate of healing among them in Fig. 7 (b-c). On days 1 and 7, mucosal tissue samples were collected from the oral ulcer for Hematoxylin and Eosin (HE) staining to evaluate epithelialization progress, and for CD11b staining to assess the inflammatory response.

As shown in Fig. 8 (c), the LP-20k treatment group demonstrated nearly complete epithelialization on the 7th day [74]. As depicted in Figure S18 (a), the HE staining reveals that on the seventh day, the thickness of the epithelial layer in the LP-20k group closely resembles that of the normal epithelium. This notable acceleration in ulcer healing by the LP-20k hydrogel can likely be attributed to its ability to provide protection against external forces and bacterial infection at the wound. Conversely, the Mund-heil gel displayed a minor enhancement in healing compared to the control group, resulting from brief retention of the gel on the wound.

Quantitative data obtained from the CD11b staining highlight that the LP-20k hydrogel exhibited minimal inflammation on day 1 in Fig. 8 (b-d) and Figure S18 (b). This result can be attributed to the excellent biocompatibility and effective wound closure, which prevents the infiltration of external bacteria. Additionally, the antimicrobial properties of the LP-20k hydrogel may contribute to eliminating bacteria at the initial wound, leading to mitigating inflammatory response. In summary, the LP-20k hydrogel demonstrates effective wound sealing and promotes healing within a wet, dynamic and concealed wound environment.

4. Conclusion

This study introduces a homogeneous network for producing sprayable PEG hydrogel sealants with remarkable anti-fatigue and low-swelling characteristics, suitable for clinical applications of various wounds in vivo. The homogeneous network is successfully formed by combining the spherical structure of lysozyme (LZM) with the orthotetrahedral structure of 4-arm-polyethylene glycol (4-arm-PEG), providing the hydrogel with outstanding fatigue resistance, low swelling and sustained adhesion. The rapid and simultaneous closure of multiple small notches and wide-area spraying on irregular surfaces of tissues demonstrate the potential capability of hydrogel for sealing multiple concealed wounds. In vitro experiments substantiate the hydrogel's robust wet adhesion, enabling it to keep wound closure even under cyclic underwater shearing. Furthermore, the hydrogel demonstrates commendable biocompatibility and antimicrobial properties. Well-established internal models of wet and dynamic wounds, such as porcine cardiac hemorrhage, lung air leakage and rat oral ulcers, demonstrate the hydrogel's commendable capabilities to seal leaks and promote the healing of oral ulcers, surpassing commonly employed clinical agents. This investigation tackles the problems in conventional strategies, wherein the concurrent attainment of heightened fatigue resistance and low swelling remains a formidable challenge. We expect that this study can provide a new strategy for developing advanced hydrogel sealants for wet, dynamic and concealed wound closure within practically clinical therapeutic applications.

Ethics approval and consent to participate

In vivo studies were performed in strict accordance with National Institutes of Health (NIH) guidelines for the care and use of laboratory animals (NIH Publication no. 85-23 Rev. 1985) and all procedures were approved by the Research Center for Laboratory Animals of Shanghai University of Traditional Chinese Medicine (Shanghai, China).

CRediT authorship contribution statement

Yi Zhang: Data curation, Investigation, Methodology, Resources, Software, Supervision, Writing – original draft, Writing – review & editing. **Yanjun Pan:** Data curation, Methodology, Resources, Validation. **Ronghang Chang:** Data curation, Supervision, Validation, Visualization. **Kangli Chen:** Data curation, Supervision, Validation. **Kun Wang:** Supervision, Validation, Visualization. **Haoqi Tan:** Methodology, Resources, Validation. **Meng Yin:** Data curation, Project administration, Resources, Validation. **Changsheng Liu:** Funding acquisition, Methodology, Resources, Supervision. **Xue Qu:** Data curation, Funding acquisition, Supervision, Writing – original draft, Writing – review & editing.

Declaration of competing interest

The authors declare that they have no competing interests.

Acknowledgments

This research was supported by the National key research and development program (2021YFB3800800), the National Natural Science Foundation of China (31922041, 11932012, 32171341, 82202334), the 111 Project (B14018), Excellence Project of Shanghai Municipal Health Commission (20234Z0003), the Science and Technology Innovation Project and Excellent Academic Leader Project of Shanghai Science and Technology Committee (21S31901500, 21XD1421100) are acknowledged.

Appendix A. Supplementary data

Supplementary data to this article can be found online at https://doi.org/10.1016/j.bioactmat.2023.12.002.

References

[1] Y. Liang, J. He, B. Guo, Functional hydrogels as wound dressing to enhance wound healing, ACS Nano 15 (8) (2021) 12687–12722.
[2] G.U. Ruiz-Esparza, X. Wang, X. Zhang, S. Jimenez-Vazquez, L. Diaz-Gomez, A.-M. Lavoie, et al., Nanoengineered shear-thinning hydrogel barrier for preventing postoperative abdominal adhesions, Nano-Micro Lett. 13 (1) (2021) 212.
[3] M.H. Norahan, S.C. Pedroza-González, M.G. Sánchez-Salazar, M.M. Álvarez, G. Trujillo de Santiago, Structural and biological engineering of 3D hydrogels for wound healing, Bioact. Mater. 24 (2023) 197–235.
[4] S. Bian, L. Hao, X. Qiu, J. Wu, H. Chang, G.-M. Kuang, et al., An injectable rapid-adhesion and anti-swelling adhesive hydrogel for hemostasis and wound sealing, Adv. Funct. Mater. 32 (46) (2022), 2207741.
[5] L. Zhang, Z. Bei, T. Li, Z. Qian, An injectable conductive hydrogel with dual responsive release of rosmarinic acid improves cardiac function and promotes repair after myocardial infarction, Bioact. Mater. 29 (2023) 132–150.
[6] Y. Jiang, X. Zhang, W. Zhang, M. Wang, L. Yan, K. Wang, et al., Infant skin friendly adhesive hydrogel patch activated at body temperature for bioelectronics securing and diabetic wound healing, ACS Nano 16 (6) (2022) 8662–8676.
[7] S. Tavakoli, M. Kharaziha, A. Kermanpur, H. Mokhtari, Sprayable and injectable visible-light Kappa-carrageenan hydrogel for in-situ soft tissue engineering, Int. J. Biol. Macromol. 138 (2019) 590–601.
[8] Z. Liu, W. Tang, J. Liu, Y. Han, Q. Yan, Y. Dong, et al., A novel sprayable thermosensitive hydrogel coupled with zinc modified metformin promotes the healing of skin wound, Bioact. Mater. 20 (2023) 610–626.
[9] Y. Yang, Y. Liang, J. Chen, X. Duan, B. Guo, Mussel-inspired adhesive antioxidant antibacterial hemostatic composite hydrogel wound dressing via photo-polymerization for infected skin wound healing, Bioact. Mater. 8 (2022) 341–354.
[10] C.F. Anderson, R.W. Chakroun, M.E. Grimmett, C.J. Domalewski, F. Wang, H. Cui, Collagen-binding peptide-enabled supramolecular hydrogel design for improved organ adhesion and sprayable therapeutic delivery, Nano Lett. 22 (10) (2022) 4182–4191.
[11] D.S. Yoon, Y. Lee, H.A. Ryu, Y. Jang, K.-M. Lee, Y. Choi, et al., Cell recruiting chemokine-loaded sprayable gelatin hydrogel dressings for diabetic wound healing, Acta Biomater. 38 (2016) 59–68.
[12] H. Geng, Q. Dai, H. Sun, L. Zhuang, A. Song, F. Caruso, et al., Injectable and sprayable polyphenol-based hydrogels for controlling hemostasis, ACS Appl. Bio Mater. 3 (2) (2020) 1258–1266.
[13] L.M. Stapleton, A.N. Steele, H. Wang, H. Lopez Hernandez, A.C. Yu, M.J. Paulsen, et al., Use of a supramolecular polymeric hydrogel as an effective post-operative pericardial adhesion barrier, Nat. Biomed. Eng. 3 (8) (2019) 611–620.
[14] J. Sun, H. Tan, H. Liu, D. Jin, M. Yin, H. Lin, et al., A reduced polydopamine nanoparticle-coupled sprayable PEG hydrogel adhesive with anti-infection activity for rapid wound sealing, Biomater. Sci. 8 (24) (2020) 6946–6956.
[15] J. He, Z. Zhang, Y. Yang, F. Ren, J. Li, S. Zhu, et al., Injectable self-healing adhesive pH-responsive hydrogels accelerate gastric hemostasis and wound healing, Nano-Micro Lett. 13 (1) (2021) 80.
[16] C. Cai, T. Wang, X. Han, S. Yang, C. Lai, T. Yuan, et al., In situ wound sprayable double-network hydrogel: preparation and characterization, Chin. Chem. Lett. 33 (4) (2022) 1963–1969.
[17] Y. Bu, L. Zhang, G. Sun, F. Sun, J. Liu, F. Yang, et al., Tetra-PEG based hydrogel sealants for in vivo visceral hemostasis, Adv. Mater. 31 (28) (2019), 1901580.
[18] H. Tan, D. Jin, J. Sun, J. Song, Y. Lu, M. Yin, et al., Enlisting a Traditional Chinese Medicine to tune the gelation kinetics of a bioactive tissue adhesive for fast hemostasis or minimally invasive therapy, Bioact. Mater. 6 (3) (2021) 905–917.
[19] H. Cheng, Z. Shi, K. Yue, X. Huang, Y. Xu, C. Gao, et al., Sprayable hydrogel dressing accelerates wound healing with combined reactive oxygen species-scavenging and antibacterial abilities, Acta Biomater. 124 (2021) 219–232.
[20] L. Li, X. Cheng, Q. Huang, Y. Cheng, J. Xiao, J. Hu, Sprayable antibacterial hydrogels by simply mixing of aminoglycoside antibiotics and cellulose nanocrystals for the treatment of infected wounds, Adv. Healthcare Mater. 11 (20) (2022), 2201286.
[21] W. Ma, H. Ma, P. Qiu, H. Zhang, Z. Yang, B. Ma, et al., Sprayable β-FeSi2 composite hydrogel for portable skin tumor treatment and wound healing, Biomaterials 279 (2021), 121225.

[22] N. Annabi, D. Rana, E. Shirzaei Sani, R. Portillo-Lara, J.L. Gifford, M.M. Fares, et al., Engineering a sprayable and elastic hydrogel adhesive with antimicrobial properties for wound healing, Biomaterials 139 (2017) 229–243.
[23] J.H.M. Wong, R.P.T. Tan, J.J. Chang, B.Q.Y. Chan, X. Zhao, J.J.W. Cheng, et al., Injectable hybrid-crosslinked hydrogels as fatigue-resistant and shape-stable skin depots, Biomacromolecules 23 (9) (2022) 3698–3712.
[24] X. Xia, Q. Liang, X. Sun, D. Yu, X. Huang, S.M. Mugo, et al., Intrinsically electron conductive, antibacterial, and anti-swelling hydrogels as implantable sensors for bioelectronics, Adv. Funct. Mater. 32 (48) (2022), 2208024.
[25] Y.S. Zhang, A. Khademhosseini, Advances in engineering hydrogels, Science 356 (6337) (2017), eaaf3627.
[26] J. Goding, C. Vallejo-Giraldo, O. Syed, R. Green, Considerations for hydrogel applications to neural bioelectronics, J. Mater. Chem. B 7 (10) (2019) 1625–1636.
[27] A. Ghoorchian, J.R. Simon, B. Bharti, W. Han, X. Zhao, A. Chilkoti, et al., Bioinspired reversibly cross-linked hydrogels comprising polypeptide micelles exhibit enhanced mechanical properties, Adv. Funct. Mater. 25 (21) (2015) 3122–3130.
[28] H. Asai, M. Shibata, M. Takenaka, S. Takata, K. Hiroi, M. Ouchi, et al., Micelle-crosslinked hydrogels with stretchable, self-healing, and selectively adhesive properties: random copolymers work as dynamic yet self-sorting domains, Aggregate 4 (3) (2023) e316.
[29] L. Fu, L. Li, Q. Bian, B. Xue, J. Jin, J. Li, et al., Cartilage-like protein hydrogels engineered via entanglement, Nature 618 (7966) (2023) 740–747.
[30] J. Kim, G. Zhang, M. Shi, Z. Suo, Fracture, fatigue, and friction of polymers in which entanglements greatly outnumber cross-links, Science 374 (6564) (2021) 212–216.
[31] P. Ge, Q. Cai, H. Zhang, X. Yao, W. Zhu, Full poly(ethylene glycol) hydrogels with high ductility and self-recoverability, ACS Appl. Mater. Interfaces 12 (33) (2020) 37549–37560.
[32] X. Huang, S. Nakagawa, X. Li, M. Shibayama, N. Yoshie, A simple and versatile method for the construction of nearly ideal polymer networks, Angew Chem. Int. Ed. Engl. 59 (24) (2020) 9646–9652.
[33] X. Li, S. Nakagawa, Y. Tsuji, N. Watanabe, M. Shibayama, Polymer gel with a flexible and highly ordered three-dimensional network synthesized via bond percolation, Sci. Adv. 5 (12) (2019), eaax8647.
[34] Y. Li, P. Yu, J. Wen, H. Sun, D. Wang, J. Liu, et al., Nanozyme-based stretchable hydrogel of low hysteresis with antibacterial and antioxidant dual functions for closely fitting and wound healing in movable parts, Adv. Funct. Mater. 32 (13) (2022), 2110720.
[35] D. Fu, G. Huang, Y. Xie, M. Zheng, J. Feng, K. Kan, et al., Novel uracil-functionalized poly(ionic liquid) hydrogel: highly stretchable and sensitive as a direct wearable ionic skin for human motion detection, ACS Appl. Mater. Interfaces 15 (8) (2023) 11062–11075.
[36] P. Liu, Y. Zhang, Y. Guan, Y. Zhang, Peptide-Crosslinked, highly entangled hydrogels with excellent mechanical properties but ultra-low solid content, Adv. Mater. 35 (13) (2023), 2210021.
[37] O.P. Nwammuo, G.C. Maitland, Effects of chain flexibility on polymer solution dynamics, J. Chem. Soc., Faraday Trans. 88 (13) (1992) 1803–1818.
[38] G. Nian, J. Kim, X. Bao, Z. Suo, Making highly elastic and tough hydrogels from doughs, Adv. Mater. 34 (50) (2022), 2206577.
[39] L. Zhang, W. Ma, T. Huaguo, Y. Yu, L. Wang, T. Li, et al., Tough, low-friction and homogeneous physical hydrogel by a solvent-inducted strategy, Chem. Eng. J. 466 (2023), 143195.
[40] M. Shibayama, Structure-mechanical property relationship of tough hydrogels, Soft Matter 8 (31) (2012) 8030–8038.
[41] C. Yang, T. Yin, Z. Suo, Polyacrylamide hydrogels. I. Network imperfection, J. Mech. Phys. Solid. 131 (2019) 43–55.
[42] T. Matsunaga, T. Sakai, Y. Akagi, U-i Chung, M. Shibayama, SANS and SLS studies on tetra-arm PEG gels in as-prepared and swollen states, Macromolecules 42 (16) (2009) 6245–6252.
[43] T. Sakai, Y. Akagi, T. Matsunaga, M. Kurakazu, U-i Chung, M. Shibayama, Highly elastic and deformable hydrogel formed from tetra-arm polymers, Macromol. Rapid Commun. 31 (22) (2010) 1954–1959.
[44] Y. Akagi, T. Matsunaga, M. Shibayama, U-i Chung, T. Sakai, Evaluation of topological defects in tetra-PEG gels, Macromolecules 43 (1) (2010) 488–493.
[45] K. Urayama, T. Kawamura, S. Kohjiya, Structure–mechanical property correlations of model siloxane elastomers with controlled network topology, Polymer 50 (2) (2009) 347–356.
[46] W. Kuhn, Dependence of the average transversal on the longitudinal dimensions of statistical coils formed by chain molecules, J. Polym. Sci. Polym. Chem. 1 (5) (1946) 380–388.
[47] H. Ren, Z. Zhang, X. Cheng, Z. Zou, X. Chen, C. He, Injectable, self-healing hydrogel adhesives with firm tissue adhesion and on-demand biodegradation for sutureless wound closure, Sci. Adv. 9 (33) (2023), eadh4327.
[48] Z. Xu, C. Fan, Q. Zhang, Y. Liu, C. Cui, B. Liu, et al., A self-thickening and self-strengthening strategy for 3D printing high-strength and antiswelling supramolecular polymer hydrogels as meniscus substitutes, Adv. Funct. Mater. 31 (18) (2021), 2100462.
[49] V. Delplace, P.E.B. Nickerson, A. Ortin-Martinez, A.E.G. Baker, V.A. Wallace, M. S. Shoichet, Nonswelling, ultralow content inverse electron-demand diels–alder hyaluronan hydrogels with tunable gelation time: synthesis and in vitro evaluation, Adv. Funct. Mater. 30 (14) (2020), 1903978.
[50] H. Zhou, S. Zhang, M. Lei, Y. Cai, H. Wang, J. Sun, et al., A suture-free, shape self-adaptive and bioactive PEG-Lysozyme implant for Corneal stroma defect repair and rapid vision restoration, Bioact. Mater. 29 (2023) 1–15.
[51] R. Diamond, Real-space refinement of the structure of hen egg-white lysozyme, J. Mol. Biol. 82 (3) (1974) 371–391.
[52] H. Tan, D. Jin, X. Qu, H. Liu, X. Chen, M. Yin, et al., A PEG-Lysozyme hydrogel harvests multiple functions as a fit-to-shape tissue sealant for internal-use of body, Biomaterials 192 (2019) 392–404.
[53] T. Chen, Y. Wang, J. Xie, X. Qu, C. Liu, Lysozyme amyloid fibril-integrated PEG injectable hydrogel adhesive with improved antiswelling and antibacterial capabilities, Biomacromolecules 23 (3) (2022) 1376–1391.
[54] W. Zhang, B. Bao, F. Jiang, Y. Zhang, R. Zhou, Y. Lu, et al., Promoting oral mucosal wound healing with a hydrogel adhesive based on a phototriggered S-nitrosylation coupling reaction, Adv. Mater. 33 (48) (2021), 2105667.
[55] K. Azuma, M. Nishihara, H. Shimizu, Y. Itoh, O. Takashima, T. Osaki, et al., Biological adhesive based on carboxymethyl chitin derivatives and chitin nanofibers, Biomaterials 42 (2015) 20–29.
[56] V. Engkagul, A. Sereemaspun, S. Chirachanchai, One pot preparation of chitosan/hyaluronic acid-based triple network hydrogel via in situ click reaction, metal coordination and polyion complexation in water, Carbohydr. Polym. 200 (2018) 616–623.
[57] S. Bang, Y.-G. Ko, W.I. Kim, D. Cho, W.H. Park, O.H. Kwon, Preventing postoperative tissue adhesion using injectable carboxymethyl cellulose-pullulan hydrogels, Int. J. Biol. Macromol. 105 (2017) 886–893.
[58] H. Ye, Y. Xian, S. Li, C. Zhang, D. Wu, In situ forming injectable γ-poly(glutamic acid)/PEG adhesive hydrogels for hemorrhage control, Biomater. Sci. 10 (15) (2022) 4218–4227.
[59] M. Shibayama, K. Nishi, T. Hiroi, Gelation kinetics and polymer network dynamics of homogeneous tetra-PEG gels, Macromol. Symp. 348 (1) (2015) 9–13.
[60] X. Meng, Y. Qiao, C. Do, W. Bras, C. He, Y. Ke, et al., Hysteresis-Free nanoparticle-reinforced hydrogels, Adv. Mater. 34 (7) (2022), 2108243.
[61] J. Li, K. Wang, J. Wang, Y. Yuan, H. Wu, High-tough hydrogels formed via Schiff base reaction between PAMAM dendrimer and Tetra-PEG and their potential as dual-function delivery systems, Mater. Today Commun. 30 (2022), 103019.
[62] X. Kuang, M.O. Arıcan, T. Zhou, X. Zhao, Y.S. Zhang, Functional tough hydrogels: design, processing, and biomedical applications, Acc. Mater. Res. 4 (2) (2023) 101–114.
[63] T. Sakai, T. Matsunaga, Y. Yamamoto, C. Ito, R. Yoshida, S. Suzuki, et al., Design and fabrication of a high-strength hydrogel with ideally homogeneous network structure from tetrahedron-like macromonomers, Macromolecules 41 (14) (2008) 5379–5384.
[64] S.F. Edwards, T.A. Vilgis, The tube model theory of rubber elasticity, Rep. Prog. Phys. 51 (2) (1988) 243.
[65] R. Feiner, T. Dvir, Tissue–electronics interfaces: from implantable devices to engineered tissues, Nat. Rev. Mater. 3 (1) (2017), 17076.
[66] X.-Y. Liu, H. Xu, L.-Q. Zhang, M. Zhong, X.-M. Xie, Homogeneous and real super tough multi-bond network hydrogels created through a controllable metal ion permeation strategy, ACS Appl. Mater. Interfaces 11 (45) (2019) 42856–42864.
[67] J. Chen, Z. Dong, M. Li, X. Li, K. Chen, P. Yin, Ultra-strong and proton conductive aqua-based adhesives from facile blending of polyvinyl alcohol and tungsten oxide clusters, Adv. Funct. Mater. 32 (33) (2022), 2111892.
[68] Y. Hou, Y. Li, Y. Li, D. Li, T. Guo, X. Deng, et al., Tuning water-resistant networks in mussel-inspired hydrogels for robust wet tissue and bioelectronic adhesion, ACS Nano 17 (3) (2023) 2745–2760.
[69] X. Chen, H. Yuk, J. Wu, C.S. Nabzdyk, X. Zhao, Instant tough bioadhesive with triggerable benign detachment, Proc. Natl. Acad. Sci. USA 117 (27) (2020) 15497–15503.
[70] He H, Qin Q, Xu F, Chen Y, Rao S, Wang C, et al. Oral polyphenol-armored nanomedicine for targeted modulation of gut microbiota–brain interactions in colitis. Sci. Adv..9(21):eadf3887..
[71] R.J. Lamont, H. Koo, G. Hajishengallis, The oral microbiota: dynamic communities and host interactions, Nat. Rev. Microbiol. 16 (12) (2018) 745–759.
[72] R. Yu, M. Li, Z. Li, G. Pan, Y. Liang, B. Guo, Supramolecular thermo-contracting adhesive hydrogel with self-removability simultaneously enhancing noninvasive wound closure and MRSA-infected wound healing, Adv. Healthcare Mater. 11 (13) (2022), 2102749.
[73] C.-Y. Zou, X.-X. Lei, J.-J. Hu, Y.-L. Jiang, Q.-J. Li, Y.-T. Song, et al., Multi-crosslinking hydrogels with robust bio-adhesion and pro-coagulant activity for first-aid hemostasis and infected wound healing, Bioact. Mater. 16 (2022) 388–402.
[74] J.H. Ryu, J.S. Choi, E. Park, M.R. Eom, S. Jo, M.S. Lee, et al., Chitosan oral patches inspired by mussel adhesion, J. Contr. Release 317 (2020) 57–66.